

Review of Raman spectroscopy of two-dimensional magnetic van der Waals materials

Yu-Jia Sun(孙宇伽), Si-Min Pang(庞思敏), and Jun Zhang(张俊)

Citation: Chin. Phys. B, 2021, 30 (**11**): 117104. DOI: 10.1088/1674-1056/ac1e0f
Journal homepage: http://cpb.iphy.ac.cn; http://iopscience.iop.org/cpb

What follows is a list of articles you may be interested in

Influence of thickness on current-induced magnetization switching in $L1_0$-FePt single layer

Shi-Qi Zheng(郑诗琪), Kang-Kang Meng(孟康康), Zhen-Guo Fu(付振国), Ji-Kun Chen(陈吉堃), Jun Miao(苗君), Xiao-Guang Xu(徐晓光), and Yong Jiang(姜勇)

Chin. Phys. B, 2021, 30 (**10**): 107101. DOI: 10.1088/1674-1056/ac0a62

Recent progress on excitation and manipulation of spin-waves in spin Hall nano-oscillators

Liyuan Li(李丽媛), Lina Chen(陈丽娜), Ronghua Liu(刘荣华), and Youwei Du(都有为)

Chin. Phys. B, 2020, 29 (**11**): 117102. DOI: 10.1088/1674-1056/abaed5

Effects of shape and dopant on structural, optical absorption, Raman, and vibrational properties of silver and copper quantum clusters：A density functional theory study

Li Wei-Yin, Chen Fu-Yi

Chin. Phys. B, 2014, 23 (**11**): 117103. DOI: 10.1088/1674-1056/23/11/117103

Characterization of deep acceptor level in as-grown ZnO thin film by molecular beam epitaxy

M. Asghar, K. Mahmood, M. A. Hasan, I. T. Ferguson, R. Tsu, M. Willder

Chin. Phys. B, 2014, 23 (**9**): 097101. DOI: 10.1088/1674-1056/23/9/097101

Growth of monodisperse nanospheres of $MnFe_2O_4$ with enhanced magnetic and optical properties

M. Yasir Rafique, Pan Li-Qing, Qurat-ul-ain Javed, M. Zubair Iqbal, Qiu Hong-Mei, M. Hassan Farooq, Guo Zhen-Gang, M. Tanveer

Chin. Phys. B, 2013, 22 (**10**): 107101. DOI: 10.1088/1674-1056/22/10/107101

TOPICAL REVIEW — Two-dimensional magnetic materials and devices

Review of Raman spectroscopy of two-dimensional magnetic van der Waals materials*

Yu-Jia Sun(孙宇伽)[1,2], Si-Min Pang(庞思敏)[1,2], and Jun Zhang(张俊)[1,2,3,4,†]

[1] State Key Laboratory of Superlattices and Microstructures, Institute of Semiconductors, Chinese Academy of Sciences, Beijing 100083, China
[2] Center of Materials Science and Optoelectronics Engineering, University of Chinese Academy of Sciences, Beijing 100049, China
[3] CAS Center of Excellence in Topological Quantum Computation, University of Chinese Academy of Sciences, Beijing 100049, China
[4] Beijing Academy of Quantum Information Science, Beijing 100193, China

(Received 28 April 2021; revised manuscript received 23 July 2021; accepted manuscript online 17 August 2021)

Ultrathin van der Waals (vdW) magnets provide a possibility to access magnetic ordering in the two-dimensional (2D) limit, which are expected to be applied in the spintronic devices. Raman spectroscopy is a powerful characterization method to investigate the spin-related properties in 2D vdW magnets, including magnon and spin–lattice interaction, which are hardly accessible by other optical methods. In this paper, the recent progress of various magnetic properties in 2D vdW magnets studied by Raman spectroscopy is reviewed, including the magnetic transition, spin-wave, spin–lattice interaction, symmetry tuning induced by spin ordering, and nonreciprocal magneto-phonon Raman scattering.

Keywords: two-dimensional (2D) magnets, Raman spectroscopy, magnon, spin–lattice interaction

PACS: 71.70.Ej, 33.20.Fb, 07.55.Db, 72.10.Di **DOI:** 10.1088/1674-1056/ac1e0f

1. Introduction

Since the successful preparation of monolayer (1L) graphene, new families of two-dimensional (2D) van der Waals (vdW) materials, including hexagonal boron nitride (h-BN), black phosphorus (BP), and transition metal dichalcogenides (TMDCs) have been discovered.[1] In recent years, the 2D vdW materials have attracted great interest due to their unique properties that are difficult to be accessed in their bulk crystal form.[1–6] Remarkably, among all the 2D vdW materials, 2D vdW magnets have gained extensive attention because they are ideal systems for studying the 2D magnetism.[7–10] Additionally, the 2D vdW magnets exhibit many fascinating electrical and optical properties, such as ultrafast optical response, magnetoresistance effect, high-frequency spin waves, and linear dichroism.[11–16] The long-range magnetic ordering in some 2D vdW magnets, such as CrI_3, $Cr_2Ge_2Te_6$, and $FePS_3$, depends on the number of layers and can be retained down to the 1L limit.[17–19] In the 2D limit, the magnetic properties are substantially different from those in their bulk counterparts, such as the existing skyrmions, spin–phonon coupling, spin fluctuations, and magnetic excitations in 2D vdW magnets.[18,20,21] Furthermore, the magnetism of 2D vdW materials can be effectively modulated by electrostatic gating, chemical doping, and epitaxial strain.[13,22,23]

The magnetism of 2D vdW materials can be characterized by some optical methods, including Raman spectroscopy, second harmonic generation (SHG), magnetic force microscope (MFM), magnetic circular dichroism (MCD), and magneto-optic Kerr effect (MOKE).[9,13,24,25] Among the various methods mentioned above, Raman spectroscopy is indispensable for the characterization of elementary excitations in 2D vdW magnets. Utilizing the Raman spectroscopy, rich information about the spin-related elementary excitations can be obtained, including magnons, spin–phonon coupling, and Brillouin zone folding.[17,21,26,27] Additionally, the different stacking orders in vdW magnets can also be distinguished by Raman spectroscopy, which is significant for the study of the layer-dependent magnetism.[12,28] Due to the atomic thickness, 2D magnets are susceptible to the external perturbations. Therefore, the response of Raman spectra to the external perturbation allows the deeper insight into the magnetic ordering.[13,29]

In this paper, some important advances of Raman spectroscopy applied in investigating the properties of 2D vdW magnets are reviewed. Firstly, we briefly summarize the atomic structures and magnetic properties of some vdW magnets. Subsequently, we introduce the ways to detect the magnetic phase transition by Raman spectroscopy. The Curie temperature (T_C) and Néel temperature (T_N) of 2D magnets can be obtained from the evolution of the Raman spectral features (including frequency, intensity, and the number of Raman peaks) with temperature. We also illustrate the Raman spectral features of spin-wave (magnon) under various conditions, including external magnetic field, low-temperature, and different polarization configurations. Next, we present

*Project supported by Beijing Natural Science Foundation, China (Grant No. JQ18014), the National Natural Science Foundation of China (Grant No. 12074371), Strategic Priority Research Program of Chinese Academy of Sciences (Grant No. XDB28000000), and CAS Interdisciplinary Innovation Team.

†Corresponding author. E-mail: zhangjwill@semi.ac.cn

© 2021 Chinese Physical Society and IOP Publishing Ltd

the strategies regarding how to use the Raman spectroscopy to monitor the magnetism which is modulated by the magnetic (electric) field, pressure, and chemical methods. Furthermore, we elucidate two mechanisms about the rotation of the polarization axis of A_g mode with the magnetic field in CrI_3. At the end of the review, we give a conclusion and brief perspective for the development directions of the Raman spectroscopy in investigating the 2D magnets in the future.

2. The 2D vdW magnets in atomically thin limit

The atomic structures and magnetic properties of several typical vdW antiferromagnetic (AFM) and ferromagnetic (FM) materials are introduced here, including ternary tetradymite compounds, ternary iron-based tellurides, transition metal halides, and transition metal phosphorous trisulfides.

Mn-Bi-Te family is a layered ternary tetradymite compound containing long-range magnetic ordering introduced by Mn^{2+} ions and the band inversion caused by the strong coupling between spin and orbit, so it is one of the ideal candidates for magnetic topological materials.[32,33] The basic building blocks of the Mn-Bi-Te family are magnetic compound $MnBi_2Te_4$ (A layer) and non-magnetic compound Bi_2Te_3 (B layer). So far, many structures can be obtained by stacking A layer and B layer experimentally, such as $MnBi_2Te_4$, $MnBi_4Te_7$, $MnBi_6Te_{10}$, and $MnBi_8Te_{13}$.[34] Recently, the intrinsic vdW AFM $MnBi_2Te_4$ has aroused widespread attention for its implementation of Chern insulator state.[33] In the layered $MnBi_2Te_4$ with the space group $R\bar{3}m$, septuple layers (SLs) Te-Bi-Te-Mn-Te-Bi-Te are bundled via vdW interaction, as shown in Fig. 1(a).[12] The Néel temperature (T_N) of $MnBi_2Te_4$ is 25 K. In the AFM phase ($T < T_N$), the spins of Mn^{2+} ions in each SL couple ferromagnetically, while SLs couple antiferromagnetically along the out-of-plane easy axis. By applying a magnetic field, $MnBi_2Te_4$ can further form canted AFM and FM states.[35] Its layered AFM order enables different topological states associated with even and odd layers, which has been supported by edge transport measurement.[36]

The Fe_3GeTe_2 (FGT), as a representative of ternary iron-based tellurides, exhibits robust long-range ferromagnetic ordering with strong out-of-plane anisotropy in monolayer and epitaxial grown thin films.[30,37,38] As shown in Fig. 1(b), with the space group $P6_3/mmc$, each layer of FGT is composed of five sublayers with sandwich-like stacking order and the adjacent layers interact through vdW force. The Curie temperature (T_C) of monolayer FGT is around 130 K,[30] while it reaches up to about 220–230 K for bulk FGT. More importantly, the bulk vdW magnet Fe_5GeTe_2, with a similar structure to Fe_3GeTe_2, possesses a higher T_C of about 310 K.[39] By changing the ratio of elements, number of layers, and external gating, the magnetic properties of FGT can be modulated, which renders it a potential material for the application in spintronic devices.[25,40,41]

Transition metal halides mainly contain MX_2 and MX_3 (M = Mn, V, Cr, Co, Fe, Ru, Ni; X = I, Cl, Br). Their magnetic properties strongly depend on the number of layers, by varying of which, the magnetic ground state can be correspondingly modified. In CrI_3, one of the typical transition metal halides, its bulk crystal displays Ising ferromagnetism below the T_C (61 K) with the spins orienting along the out-of-plane direction, as shown in Figs. 1(c) and 1(d). The exfoliated monolayer retains long-range ferromagnetic order when CrI_3 is cooled below its T_C of 45 K.[9,42] In CrI_3 flakes ($\geq$ 2 L), the magnetism in a single-layer component is FM, while the coupling between adjacent layers is AFM.[43]

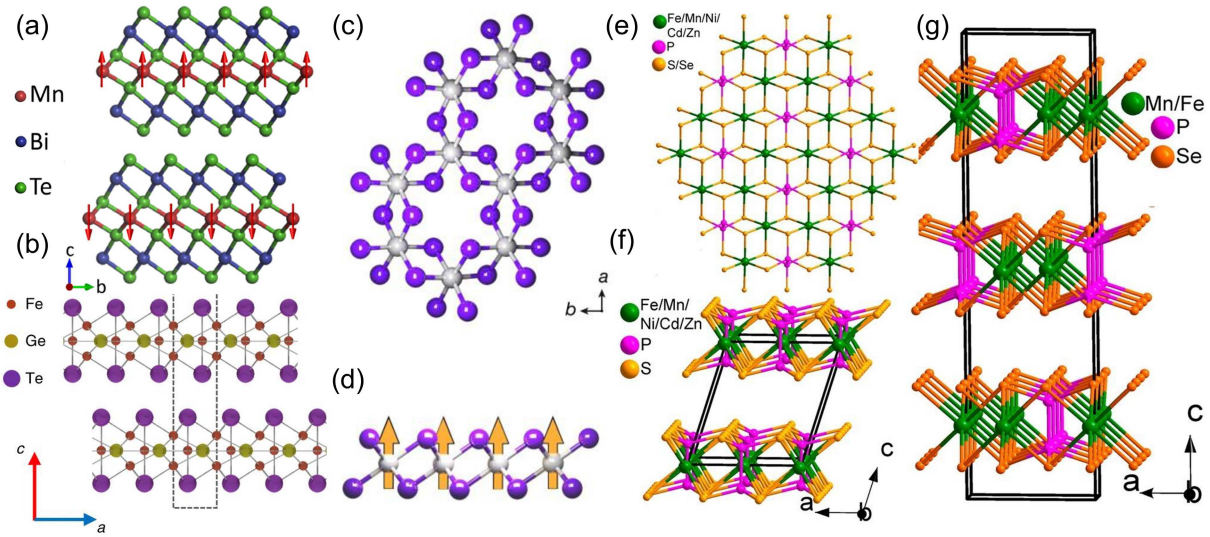


Fig. 1. Atomic structure diagrams of some typical 2D magnetic materials. (a) Crystal lattice and spin structure of $MnBi_2Te_4$. The red arrow indicates the magnetic moment of each Mn ion (adapted from Ref. [12]). (b) Side view of Fe_3GeTe_2 bilayer atomic structure. The dashed box represents the crystal unit cell (adapted from Ref. [30]). (c)–(d) The top and side views of atomic lattice and Ising spin structure of 1L CrI_3. Each Cr^{3+} ion (gray ball) is surrounded by six I^- ions (purple balls) (adapted from Ref. [9]). (e) The atomic structure of transition metal phosphorus trisulfides (adapted from Ref. [31]). The crystal structures of (f) MPS_3 (M = Mn, Fe, Ni, Cd, and Zn) and (g) $MPSe_3$ (M = Mn and Fe).

Moreover, the transformation of the magnetic orders between FM and AFM states has been realized by controlling the stacking, magnetic field, pressure, and electric gating, which provides the possibility to design highly tunable spintronics devices and even create new quantum states in 2D magnets.

Transition metal phosphorus trisulfides MPX_3 (M = Mn, Fe, Ni, etc.; X = S and Se) are another class of vdW antiferromagnets studied in the 2D limit.[31,44,45] As shown in Figs. 1(e)–1(g), each $[P_2X_6]^{4-}$ unit within a layer is surrounded by six metal ions, forming a honeycomb structure.[31] The space group of MPS_3 is $C2/m$, while $MPSe_3$ belongs to $R\bar{3}$ space group.[31] By selecting different elements, the band gaps of MPX_3 can be tuned in the range of 1.3–3.5 eV with their spin structures varying dramatically. In the bulk form, the spin model of $FePS_3$ ($T_N \approx 120$ K) belongs to the Ising model,[46] while the one for $MnPS_3$ ($T_N \approx 78$ K) is the Heisenberg model,[26] for $NiPS_3$ ($T_N \approx 155$ K) is the XY model.[27,47] In addition, the one-magnon scattering in $FePS_3$[21] and $MnPS_3$,[48] together with the two-magnon scattering in $NiPS_3$[27] have been revealed, which suggests that they have potential in magnon-based spintronic devices.

3. Raman spectroscopy of 2D magnets

3.1. Principle of Raman spectroscopy

As a convenient and non-destructive tool with high spatial and spectral resolution, Raman spectroscopy has been widely used to characterize 2D materials.[49–56] The prominent features of Raman peaks, including frequency, full width at half maximum (FWHM), intensity, and line shape, contain useful information to investigate the fundamental physical properties of 2D materials, such as phonon frequency, the number of layers, stacking orders, electron–phonon coupling, charge density wave (CDW), phase transition, *et al.*[57–60]

The quantum picture of the inelastic Raman scattering process can be understood as shown in Fig. 2(a).[61] Raman scattering describes the interaction between photons and phonons. Electrons are excited by the incident photons from the initial state to the intermediate state through electron–radiation interaction, and then scattered by phonons accompanied by the emission of scattered photons. According to the creation or annihilation of phonons, Raman process can be divided into Stokes and anti-Stokes processes. In the Stokes (anti-Stokes) process, the energy of the scattered light satisfies $\hbar\omega_{S(AS)} = \hbar\omega_i \mp \hbar\omega_{ph}$, where $\hbar\omega_i$ ($\hbar\omega_{ph}$) is the energy of the incident light (phonon) and $\hbar\omega_{S(AS)}$ is the energy of the Stokes (anti-Stokes) light. Especially, if the intermediate state is a real electronic state, the energy of the incident or scattered light will resonant with the energy of the intermediate real electronic level, and thus the resonant Raman scattering occurs. Since the real electronic transition is involved, many novel phenomena can be investigated by resonant Raman scattering, including the breakdown of Raman selection rules,[62] forbidden Raman modes,[63] high order or combined Raman modes.[63] Experimentally, the resonance Raman scattering can be achieved by either selecting the excitation energy or changing the electronic levels.

Inelastic light scattering provides access to explore the energy, symmetry and statistics of lattice, electronic excitations, and magnetic excitations in nanomaterials. Through spin–orbit and spin–lattice couplings, Raman scattering can measure various magnetic excitations, including fluctuations of the magnetic energy density, spin-orders, spin-related symmetry and topology, magnons, and spinons (fractional magnons expected in frustrated systems). For example, the transition from paramagnetic phase to antiferromagnetic phase could result in the unit cell associated with the antiparallel spin arrangement becoming twice as large as that with paramagnetic order.[17] Correspondingly, the Brillouin region of the antiferromagnetic phase would fold to half as large as that of the paramagnetic phase. Therefore, the frequencies of the relevant Raman modes would exhibit an abrupt shift or the new Raman modes would be activated. Concerning some ferromagnetic materials, the symmetry of Raman tensor changes when the time-reversal symmetry is broken near the Curie temperature, which suggests that temperature-dependent polarized Raman spectroscopy can be used to detect the magnetic phase transition temperature.[29] As an elementary excitation,

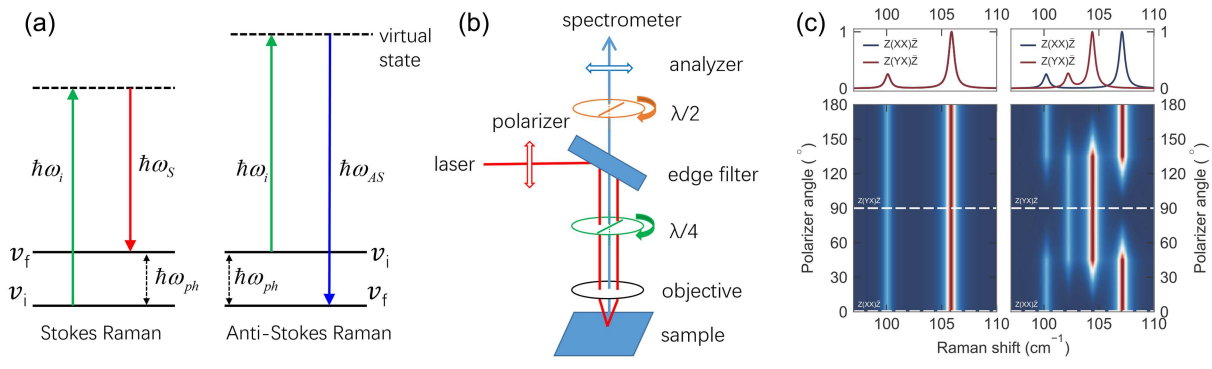


Fig. 2. Principle and application of Raman spectroscopy. (a) Schematic diagrams of energy level transitions in Stokes and anti-Stokes Raman processes. (b) Experimental setup of circularly polarized Raman spectra. (c) The intensity maps of the polarized-dependent Raman spectra in rhombohedral (left) and monoclinic (right) phases of bulk CrI_3 (adapted from Ref. [28]).

magnon originates from the collective excitation of the spins with long-range magnetic order in magnets. The energies of the one-magnon and two-magnon excitations increase when the temperature decreases, leading to the blueshift of the Raman modes.[21] Additionally, the antiferromagnetic one-magnon mode will split into two Raman peaks that vary linearly with the magnetic field due to the Zeeman effect.[21] For uncovering novel topology, Raman spectroscopy can also be used to measure the non-trivial statistics associated with the fractional spin excitations.[64]

Raman spectroscopy is widely used in both laboratory and mass-scale production. The polarization-dependent and ultralow-frequency Raman spectroscopy systems combining the polarizer, wave plate, and volume-Bragg-gratings (VBG)-based notch filter with confocal microscopes provide a powerful technique to investigate the low-energy elementary excitations, interlayer stacking, lattice symmetry, together with the anisotropy in 2D materials and heterostructures.[65,66] The polarization Raman spectroscopy, which includes linear polarization and circular polarization configurations, is available to investigate the symmetry of lattice and elementary excitations by controlling the polarization configurations of the incident and scattered light.[67–69] Figure 2(b) shows one of the experimental setups of circularly polarized Raman spectra. Since the polarized intensity can be calculated by the Raman tensor, which directly depends on the symmetry of the crystal and corresponding phonon mode, the polarization Raman spectroscopy can be used to characterize the crystal symmetry. For instance, the crystal lattice of bulk CrI_3 undergoes a structural phase transition near 210 K from a rhombohedral phase to a monoclinic phase. As shown in Fig. 2(c), the monoclinic (right) and rhombohedral (left) phases can be distinguished according to their polarization behaviors of the corresponding Raman modes.[28]

3.2. Magnetic phase transitions

The critical temperature of magnetic phase transition is an important parameter for 2D magnets, which reflects the competition between long-range magnetic order and thermal fluctuation. Most of the 2D magnets possess a low magnetic phase transition temperature, such as bulk CrI_3 ($T_C \approx 61$ K), VI_3 ($T_C \approx 50$ K), $CrSiTe_3$ ($T_C \approx 32$ K), and CrOCl ($T_N \approx 13$ K).[9,70–72] Obviously, the vdW magnets with the magnetic phase transition temperature above the room temperature are urgently demanded to achieve antiferromagnetic/ferromagnetic devices.[14] Therefore, a fast and convenient method to measure the magnetic phase transition temperature is necessary for the application of 2D magnets in spintronic devices.

The magnetic phase transition temperature of intrinsic magnets can be characterized by magnetic susceptibility measurement. However, this technique is difficult to be applied to investigate the magnetic properties of 2D ultrathin materials.[46] In contrast, due to the high spatial resolution and high sensitivity to the symmetry of the lattice, spin−phonon coupling, and electronic states, Raman spectroscopy can reveal the magnetic order and phase transitions of 2D magnets down to the monolayer limit. The comparison of the magnetic phase transition temperatures measured by Raman spectroscopy and other methods is shown in Table 1. In the vicinity of the magnetic phase transition temperature, some spectral features of Raman spectra, such as frequency, intensity, linewidth, and polarization of phonon peak, will exhibit noticeable variations, which makes the temperature-dependent Raman spectroscopy a powerful tool to determine the magnetic transition temperature of vdW magnets.[26] The related experimental results are presented in Fig. 3.

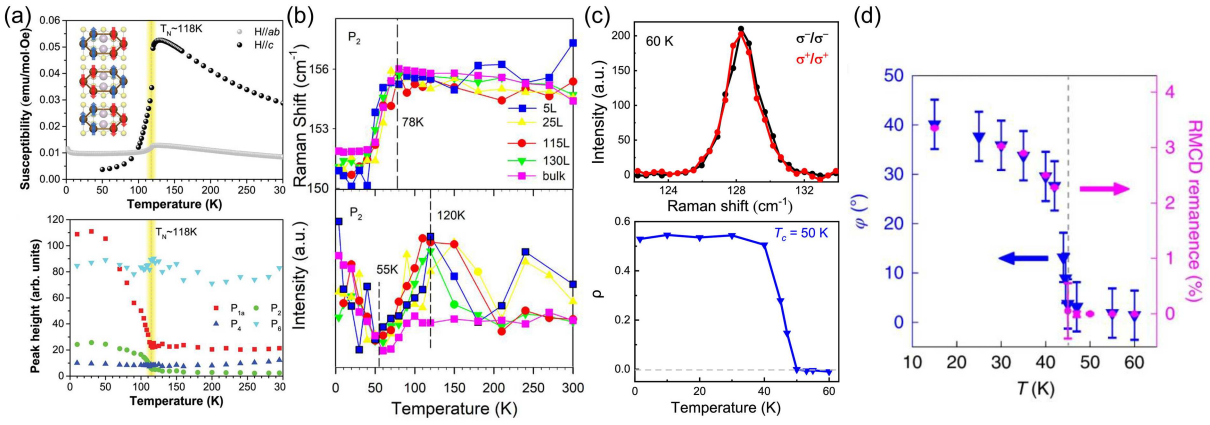


Fig. 3. The transition temperature (T_C and T_N) of 2D magnets detected by temperature-dependent Raman spectra. (a) Temperature-dependent magnetic susceptibility (upper panel) of bulk $FePS_3$ along in-plane and out-of-plane axes, depicted by gray and black spheres, respectively. The temperature-dependent intensities (lower panel) of corresponding Raman peaks in bulk $FePS_3$ (adapted from Ref. [46]). (b) Raman frequencies and intensities of P_2 in $MnPS_3$ flakes with different thickness as a function of temperature (adapted from Ref. [26]). (c) The circular polarization Raman spectra of the A_g mode (128 cm^{-1}) for bulk VI_3 under the $\sigma^{\pm}/\sigma^{\pm}$ polarization configurations at 60 K, and the corresponding calculated circular polarization (ρ) with the temperature ranging from 1.7 K to 60 K (adapted from Ref. [29]). (d) The temperature-dependent φ (blue) and the remanence RMCD signal (red) of monolayer CrI_3 at 0 T. φ is defined as the angle of the polarization axis away from the excitation polarization axis (adapted from Ref. [13]).

Table 1. Comparison of the magnetic phase transition temperatures measured by Raman spectroscopy and other methods.

VdW magnets	Magnetic phase transition temperature	
	By Raman spectroscopy	By other methods
CrI_3	—	Bulk: 61 K (magnetic susceptibility, heat capacity, and SQUID magnetometry)[9,73]
	1L : 45 K[13]	1L: 45 K (MOKE)[9]
$CrBr_3$	Bulk: 37 K[74]	Bulk: 37 K (neutron and x-ray diffraction measurements)[74]
	—	1L: 27 K (MCD)[75]
VI_3	Bulk: 50 K[29]	Bulk: 49 K (magnetic susceptibility)[76]
$CrSiTe_3$	Bulk: 33 K[77]	Bulk: 33 K (magnetic susceptibility)[77]
Fe_3GeTe_2	FLs: 140 K[78]	Bulk: 220 K (heat capacity)[79]
	—	1L: 130 K (RMCD)[30]
$FePS_3$	Bulk: 118 K[46]	Bulk: 118 K (magnetic susceptibility)[46]
	1L: 104 K[31]	—
$MnPS_3$	Bulk/FLs: 78 K[26]	Bulk: 78 K (magnetic susceptibility)[80]
$NiPS_3$	Bulk: 155 K[27]	Bulk: 155 K (magnetic susceptibility)[81]
	2L: 130 K[27]	—

Notation: 1L: monolayer, FLs: few layers, SQUID: superconducting quantum interference device, MOKE: magneto-optic Kerr effect, MCD: magnetic circular dichroism, RMCD: reflective magnetic circular dichroism.

As shown in Fig. 3(a), the slope of the magnetic susceptibility–temperature curve for $FePS_3$ exhibits a mutation when the sample undergoes the antiferromagnetic–paramagnetic phase transition, which can be exploited to determine the magnetic phase transition temperature. Meanwhile, the intensities of P_{1a} and P_2 Raman peaks vary dramatically near the T_N (118 K) obtained from the magnetic susceptibility measurement,[46] which is thus also the indicator for the magnetic phase transition. Compared with the changes of the intensity in $FePS_3$, the steep Raman shift of the P_2 peak in $MnPS_3$ (originates from the Mn–S vibration), as shown in Fig. 3(b), suggests that the transition between paramagnetic and antiferromagnetic phases occurs.[26] The temperature-dependent Raman spectra of $MnPS_3$ with different thickness indicate that the transition temperature is independent of the number of layers.[26] The Raman intensities of the P_2 mode in $MnPS_3$ with different thickness reach a maximum at around 120 K, while a minimum at around 55 K, which are related to the single-ion and XY anisotropies, respectively.

When some ferromagnetic materials undergo the paramagnetic to ferromagnetic phase transition, the time-reversal symmetry is broken due to the spin inversion, which results in an extra antisymmetric component in the original symmetric Raman tensor. The variation of the Raman tensor further induces the rotation of the polarization plane,[13] which illustrates that the transition temperature (T_C) of some ferromagnetic materials can be obtained by the polarization Raman spectroscopy. Furthermore, the circular polarization ρ can be obtained from the intensity difference of Raman mode under σ^+/σ^+ (I_+) and σ^-/σ^- (I_-) polarization configurations. Specifically, circular polarization ρ can be calculated by

$$\rho = (I_+ - I_-)/(I_+ + I_-). \quad (1)$$

Figure 3(c) shows the temperature-dependent circular polarization ρ of A_g mode (~ 128 cm^{-1}) in bulk VI_3.[29] Above T_C (50 K), the intensity of the A_g mode under σ^+/σ^+ circular configuration is the same as that under σ^-/σ^- configuration. When the temperature goes below the T_C, the spins are oriented to form ferromagnetic phase along the out-of-plane. The ordered alignment of the spins is responsible for the broken time-reversal symmetry in bulk VI_3, which manifests the appearance of asymmetric matrix elements in the Raman tensor. The circular polarization ρ of materials with FM phase is a nonzero value. In particular, ρ is positive for bulk VI_3, as shown in Fig. 3(c). Thus, *in-situ* characterization of the magnetic phase transition via circular polarization Raman spectra is available. Figure 3(d) displays the extracted polarization rotation (φ) of the A_{1g} peak in 1L CrI_3 when the temperature drops down from 60 K to 15 K. φ is defined as the angle of polarization axis away from the excitation polarization axis. When $T < T_C$ (45 K), the φ of 1L CrI_3 appears and then increases gradually as the temperature drops to 15 K.[13] The variation of φ can also be reflected in the temperature-dependent remnant RMCD signal measurement. The above experimental results indicate that the Raman spectra are considerably useful for the better understanding of the magnetic phase transition behaviors in 2D magnets.

3.3. Magnons in 2D magnets

Spin wave, whose quasiparticle is called magnon, is a collective excitation of the spins with long-range magnetic order in magnetic materials.[50] The discovery of the vdW magnets makes it possible to explore the spin dynamics when the dimension is down to the 2D limit.[50] Magnons have now been observed in several 2D magnets, including CrI_3, α-$RuCl_3$, and the MPX_3 family ($FePS_3$, $MnPS_3$, $NiPS_3$, and $MnPSe_3$),[21,27,82] which can efficiently transport the spin angular momentum and sensitively respond to the magnetic field.

The magnetic field- and temperature-dependent Raman spectroscopy is the effective and accurate method to study the properties of magnons in 2D magnets. One-magnon scattering mode in an AFM material is expected to experience the Zeeman splitting in the presence of an applied magnetic field due to its nontrivial net magnetic moment, $\Delta S = \pm 1$.[84] As shown in Fig. 4(a), the φ_4 peak of $FePS_3$ in the AFM phase splits into two peaks under the magnetic field along Z direction, which are labeled as $\varphi_4^{(1)}$ and $\varphi_4^{(2)}$, respectively, and their

frequency difference increases as the magnetic field goes from 0 T to 9 T.[21] The magnon frequency in a magnetic field exhibits a close relation with the anisotropy field (H_A), applied magnetic field (H_0), exchange field (H_E), and gyromagnetic ratio ($\gamma = \frac{g\mu_B\mu_0}{2\pi\hbar}$), which can be described as

$$\omega_{k=0} = \gamma\{(2H_E + H_A)H_A\}^{1/2} \pm \gamma H_0. \quad (2)$$

With the linear fitting, the gyromagnetic ratio $\gamma = 0.9348$ cm^{-1}/T and $g \approx 2.0023$ of $FePS_3$ can be calculated.[21] Apart from the antiferromagnetic magnon, the Raman peak of ferromagnetic magnon also shifts linearly with the applied magnetic field. As depicted in Fig. 4(d), the magnon frequency of monolayer CrI_3 shifts linearly with a slope of 0.94 cm^{-1}/T under the out-of-plane magnetic field, revealing that the magnon in 1L CrI_3 is a quasiparticle with spin $S = 1$.[50] From the magnon energy at 0 T obtained by linear fitting, the spin-wave gap around ~ 2.4 cm^{-1} is determined, which would increase with the magnetic anisotropy.

The temperature-dependent Raman spectra of $MnPSe_3$ and $NiPS_3$ under crossed polarization configuration are shown in Figs. 4(b) and 4(c). The discrete peaks correspond to the phonon modes, while the wide continuum peaks are associated with the two-magnon excitation. Unlike one-magnon peak, the two-magnon peak possesses the energy twice as large as

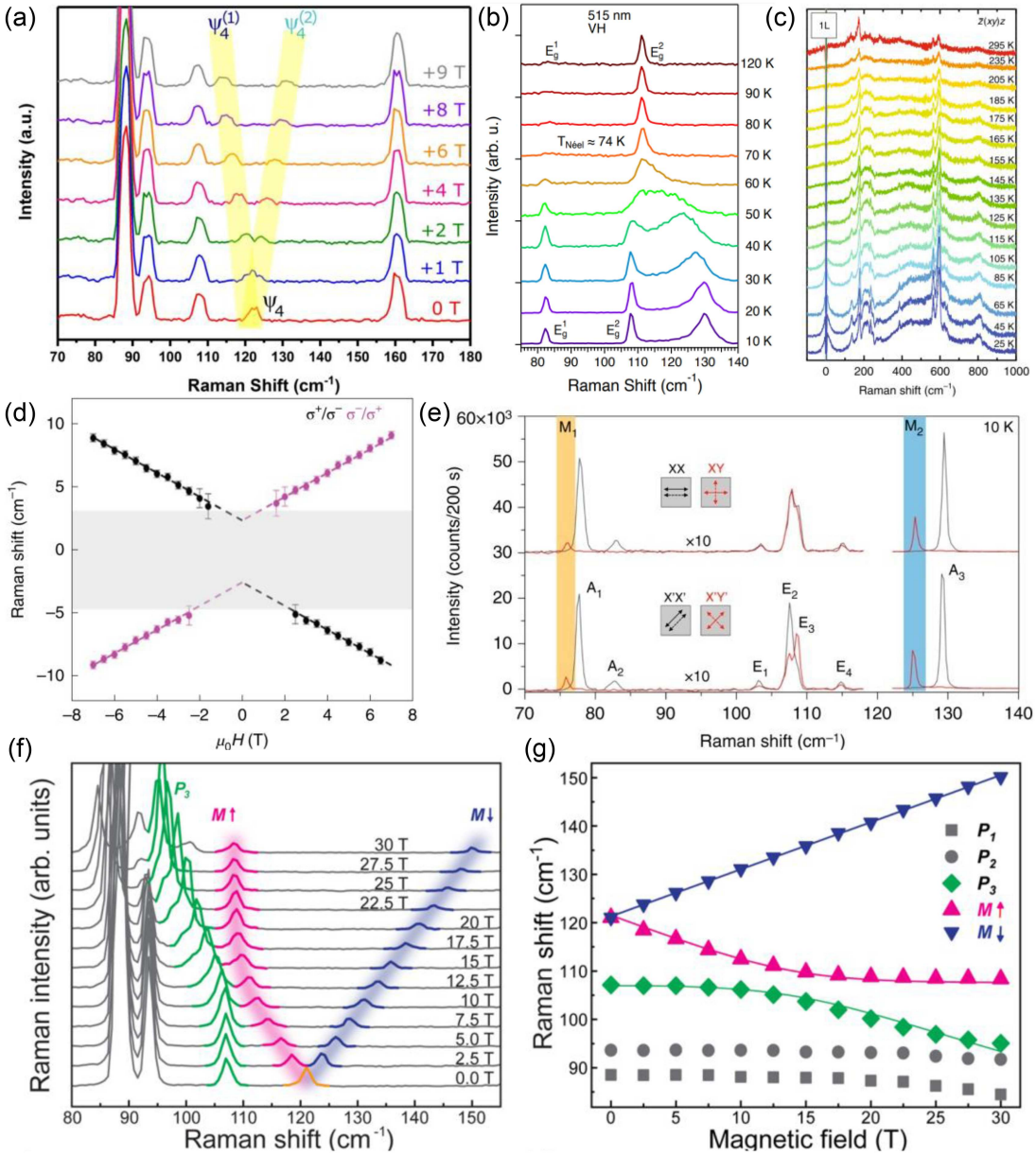


Fig. 4. Raman spectroscopy detects the one-magnon (two-magnon) in 2D magnetic materials. (a) The Zeeman splitting of ψ_4 peak in $FePS_3$ at 5 K (adapted from Ref. [21]). (b) The Raman spectra of $MnPSe_3$ under crossed (VH) polarization configuration collected through the Néel transition at 74 K (adapted from Ref. [82]). (c) Temperature-dependent Raman spectra of two-magnon signals and Fano resonance in monolayer $NiPS_3$ (adapted from Ref. [27]). (d) The magnon frequency of monolayer CrI_3 when an out-of-plane magnetic field sweeps from -7 T to $+7$ T. The working range of the filter determines that the Raman signal in the gray area is inaccessible (adapted from Ref. [50]). (e) The polarization-dependent Raman spectra of CrI_3 flake (13 L). Magnon modes M_1 and M_2 completely disappear under the parallel polarization configuration (adapted from Ref. [83]). (f) The Raman spectra of $FePS_3$ under the magnetic field along out-of-plane ranging from 0 T to 30 T (adapted from Ref. [91]). The green, red, and blue spectra correspond to phonon (P_3), spin-up magnon ($M_\uparrow$), and spin-down magnon ($M_\downarrow$), respectively. (g) The frequencies of P_1, P_2, P_3, $M_\uparrow$, and $M_\downarrow$ under the magnetic field sweeping from 0 T to 30 T (adapted from Ref. [91]). P_1, P_2, and P_3 denote three different phonon modes in $FePS_3$.

that of the one-magnon peak and would not split under the magnetic field. As the temperature decreases below the T_N, the Raman peaks of one-magnon and two-magnon show an obvious blueshift. Meanwhile, the Raman intensity of the two-magnon peak significantly increases. Similar temperature dependence of magnon has been reported in vdW magnet $FePS_3$[21] and some three-dimensional antiferromagnets, including FeF_2, NiF_2, and MnF_2.[85–88]

The symmetry behaviors of magnons can also be characterized by Raman spectroscopy. For example, in Fig. 4(e), two modes (M_1 and M_2) of thick CrI_3 can only be detected by the cross-polarization channel. According to the theory of Fleury and Loudon,[84] the Raman tensor of one-magnon peak in magnets with orbital angular momentum ground state $L = 0$ contains only the asymmetric matrix elements, which thus restricts the Raman peak to be observed only under the cross-polarization configuration, while disappears under the parallel-polarization configuration. The theory has well described the symmetry behaviors of the magnons in some 3D magnets, including antiferromagnetic materials MnF_2, FeF_2, $YFeO_3$, and $Cd_{1-x}Mn_xTe$.[84,89,90] However, the polarization behavior of one-magnon peak for magnets with the nonzero orbital angular momentum at the ground state is more complex, which is not discussed here.[21] In general, the Raman peak of two-magnon does not depend on the polarization.[27] Therefore, a suitable polarization configuration can be selected according to the polarization behaviors of the phonon modes in Raman spectra to observe the two-magnon signals. For example, two-magnon signals in $MnPSe_3$, VI_3, and $NiPS_3$ can be explored under the cross-polarization configuration because most of the phonon modes only appear under the parallel-polarization configuration.[27,29,82] Generally speaking, there is still abundant space here to explore the polarization behaviors of the magnons in the 2D limit.

The coupling between magnons and phonons in 2D antiferromagnets is an emerging field in the area of light–matter interaction, which offers a powerful means to control the quantum states and is expected to be used in quantum information technologies. Recently, Liu[91] and Vaclavkova[92] *et al.* directly observed the strong coupling between magnons and phonons in $FePS_3$ by Raman spectroscopy under the high magnetic field up to 30 T. In Figs. 4(f) and 4(g), the Raman-active magnon ($M_\uparrow$) is coupled with the nearby phonon mode (P_3) to from a hybridized magnon–phonon quasiparticle, which features an evident anti-crossing in the eigen-spectrum. In addition, the circular polarized Raman spectra shows that the magnon ($M_\uparrow$) transfers its spin to the phonon (P_3) through the strong coupling under the out-of-plane magnetic field. These works unveil the magnon polarons in $FePS_3$ and evoke further explorations in the domain of magnon–phonon coupling.

3.4. Modulation of the magnetism in 2D magnets

VdW materials are extremely flexible, and their electron density can be efficiently tuned by the electric field, leading to the fantastic transport properties. The vdW magnets provide an ideal platform to combine the magnetic properties with the unique properties of vdW materials, which makes it possible to investigate, modify the magnetic excitations, and even switch the magnetic configurations in the 2D limit. Regarding the magnetic modification, the electrical, mechanical, and chemical methods (such as elemental substitution and absorption) can be applied to modulate the magnetic properties in 2D vdW magnets.[93,94] The magnetism of vdW magnets strongly depends on the stacking order because of their ultrathin thickness. The interlayer coupling in CrI_3 with monoclinic stacking order exhibits AFM feature, while that in rhombohedral stacking order is FM. The monoclinic-to-rhombohedral (AFM–FM) transition in exfoliated 5L CrI_3 induced by pressure (1.8 GPa) has been probed by Raman spectroscopy.[51]

Compared with other vdW materials, vdW magnets have an additional degree of freedom, namely, the spin order, which can be easily tuned to control the symmetry. Below the T_C, the antisymmetric elements in the Raman tensor of

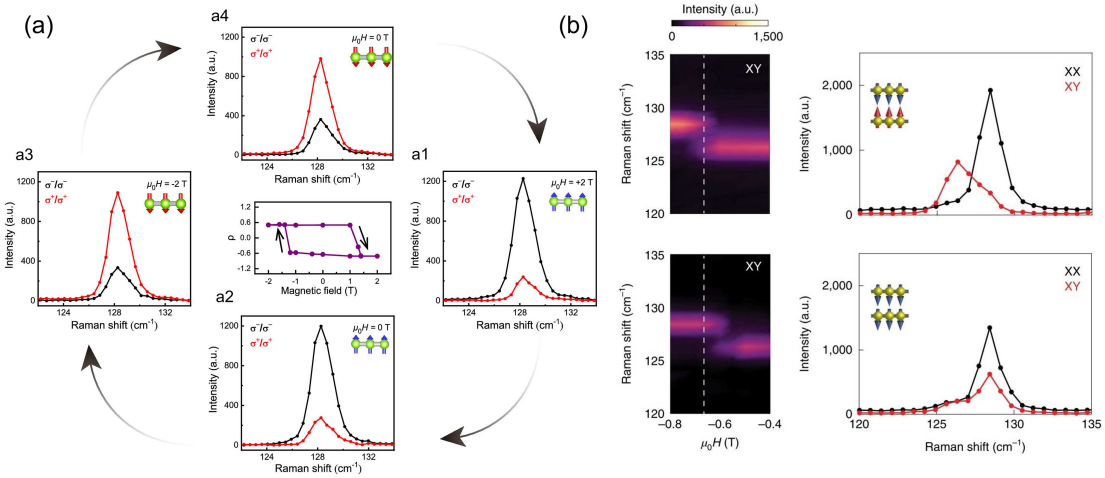


Fig. 5. Spin-dependent Raman scattering modulated by an external field in the 2D magnets. (a) The circularly polarized Raman spectra of 2D ferromagnet VI_3 under the out-of-plane magnetic field (adapted from Ref. [29]). (b) The polarized Raman spectra of 2L CrI_3 at V_g equaling to 0 V (upper panel) and 5 V (lower panel) with an applied magnetic field ranging from −0.4 T to −0.8 T (adapted from Ref. [13]). The white dotted-lines represent the spin-flip field when V_g is 0 V.

VI_3 appear due to the broken time-reversal symmetry.[29] As shown in Fig. 5(a1), when the applied magnetic field is +2 T, the intensity of A_g mode (128 cm^{-1}) under the σ^+/σ^+ circular polarization configuration is lower than that under the σ^-/σ^- configuration, which would remain unchanged when lowering the magnetic field to 0 T [Fig. 5(a2)]. However, the intensities from both channels are reversed under the opposite field of −2 T [Fig. 5(a3)], due to the spin-flip transition, which are retained when the magnetic field is back to 0 T [Fig. 5(a4)]. The reversed intensities reflect the presence of coercive field in VI_3. These results suggest that Raman selection rules are highly sensitive to the magnetism.

Being characterized by low energy consumption and ultra-scalability,[95] the electrical methods, such as applying current or voltage, can be used to control the magnetic properties in 2D vdW magnets, via changing the position of Fermi level, space inversion and time-reversal symmetries, together with the magnetic anisotropy.[14] For example, the direction of magnetic anisotropy in $CrGeTe_3$ is along the out-of-plane without applied field, whereas it rotates to in-plane with an ionic gating, and the corresponding T_C increases to above 200 K in this process.[96] As for 2L CrI_3, the symmetry can be broken by an electric field, and thus the Raman selection rules are further modified.[13] In Fig. 5(b), the Raman peak of 1L CrI_3 with frequency around 127.4 cm^{-1} splits into two peaks due to the Davydov splitting. The frequencies of these two peaks are 128.8 cm^{-1} and 126.7 cm^{-1}, respectively. According to the symmetry of vibration and Raman selection rules, the Raman peak with a higher frequency (128.8 cm^{-1}) is Raman active, while the one with lower frequency (126.7 cm^{-1}) is Raman silent in the FM phase. In the AFM state, the symmetry of bilayer CrI_3 varies, which induces that the 126.7 cm^{-1} peak can only be observed in the XY polarized channel, whereas the 128.8 cm^{-1} peak only appears under the XX configuration. As the magnetic field increases beyond the spin-flip field (−0.62 T), the bilayer CrI_3 changes from the AFM state to FM state, which can be directly reflected in the polarized Raman spectra. Figure 5(b) shows the polarized Raman spectra of 2L CrI_3 at V_g equaling to 0 V and 5 V, respectively, with an applied magnetic field changing from −0.4 T to −0.8 T. When the gate voltage V_g is 5 V, the mode at ∼ 126.7 cm^{-1} is Raman inactive under the XY configuration, while the peak at 128.8 cm^{-1} is Raman active. These results illustrate that the gate voltage can effectively control the magnetism of CrI_3 from AFM to FM state by reducing the spin-flip field, as indicated by the white dotted-lines in Fig. 5(b).

3.5. Magneto-optic effect in 2D magnets

The magneto-optic effect is a general term for a series of phenomena that light interacts with a magnetic substance (or a non-magnetic substance in a magnetic field), causing variations in the propagation state (polarization, intensity, etc.). Magneto-optic effects include the Faraday and Kerr effects, which represent the polarization changes of the transmitted and reflected light, respectively. Recently, the magnetic field has been found to be capable of inducing the polarization plane of the anisotropic mode in 2D ferromagnet CrI_3 to rotate.[97,98] The polarization Raman spectroscopy has been used to detect the anisotropic inelastic phonon scattering of CrI_3 under the external magnetic field.

As shown in Figs. 6(a) and 6(d), the A_g mode (∼ 128 cm^{-1}) of multilayered CrI_3 exhibits pronounced anisotropy with a 180° polarization period, while the E_g mode (∼ 246 cm^{-1}) is isotropic in-plane.[98] When the

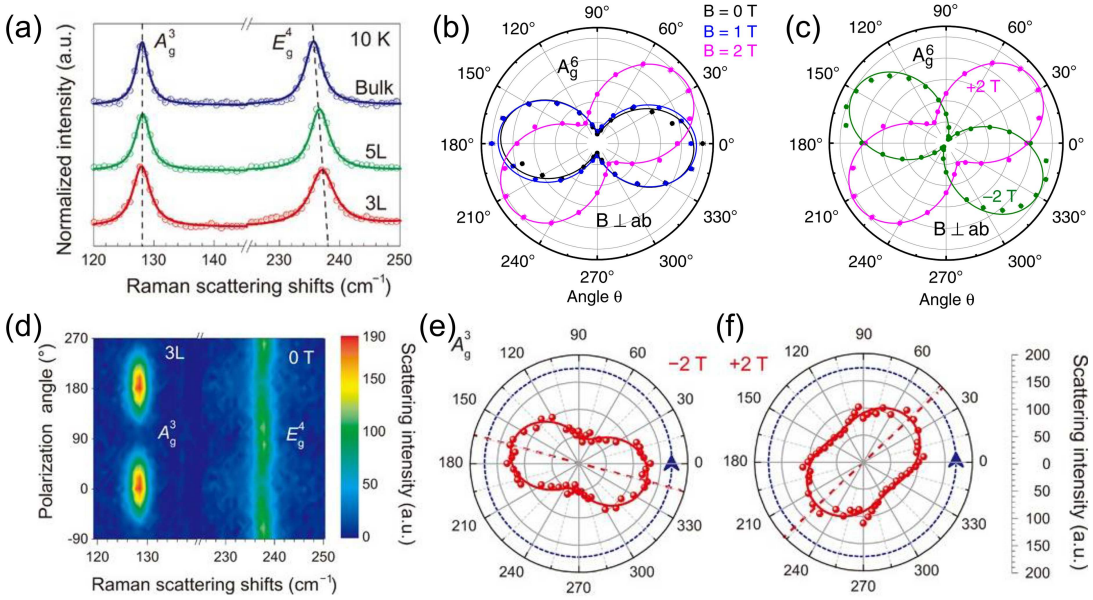


Fig. 6. The magnetic field-dependent rotation of the polarization plane in CrI_3. (a) Raman spectra of CrI_3 flakes with different thickness at 10 K (adapted from Ref. [98]). (b)–(c), (e)–(f) The magnetic field-dependent intensity of the A_g (∼ 128 cm^{-1}) mode. In (b)–(c), the polarization axis rotates the same angle under ±2 T magnetic field (adapted from Ref. [97]). In (e)–(f), the polarization axis of the A_g mode rotates −15° and 40° at −2 T and +2 T, respectively (adapted from Ref. [98]). (d) Intensity contour plot of the A_g mode of 3L CrI_3 at 0 T with the polarization of the incident light going from −90° to 270°. The red to blue colors indicate the intensity of the A_g peak varying from maximum (190) to zero (adapted from Ref. [98]).

out-of-plane magnetic field $B \geq +1.8$ T, the polarization axis of the anisotropic A_g mode rotates 35° relative to the external magnetic field direction [Figs. 6(b) and 6(c)].[97] The rotation direction of the polarization plane changes reversely with the reverse magnetic field direction, which can be explained by introducing magnetization m into the Raman tensor. The Raman tensor of A_g phonon under an out-of-plane magnetic field can be described as

$$R_{A_g,B\perp ab} = R_{A_g,m=0} + m_Z \cdot R_{A_g,m_Z}. \tag{3}$$

Due to the FM state transition and the minimal change of the point group, the Raman tensor of the A_g mode under the $+Z$ and $-Z$ magnetic fields can be expressed as

$$\begin{aligned} R_{A_g,+B_Z} &= \begin{pmatrix} \alpha & m_Z\gamma \\ -m_Z(\gamma+\Delta') & \alpha+\Delta \end{pmatrix}, \\ R_{A_g,-B_Z} &= \begin{pmatrix} \alpha & -m_Z\gamma \\ m_Z(\gamma+\Delta') & \alpha+\Delta \end{pmatrix}, \end{aligned} \tag{4}$$

respectively, where the Δ and Δ' are minor corrections. This Raman tensor of magnetization modulation well explains the polar plots for the variation of the A_g mode with the magnetic fields.

In Liu's work, as shown in Figs. 6(e) and 6(f), the polarization axis of the A_g mode in bulk CrI_3 rotates $-15°$ and 40° at -2 T and $+2$ T, respectively.[98] Moreover, the rotation angle of the polarization axis is greater than $+60°$ ($-20°$) in the presence of a higher magnetic field 2.5 T (-2.5 T). The rotation of the polarization axis originates from the regulation of the polarizability and dielectric constant exerted by the applied magnetic field. This theory starts from the dynamics of electrons under the magnetic field and then obtains the magnetic field-dependent polarizability α. Exploiting the polarizability α, the polarized Raman tensor of the A_g mode (~ 128 cm^{-1}) under the out-of-plane magnetic field B can be described as

$$\alpha_K^L\left(A_g(B)\right) = \frac{e}{\omega}\begin{bmatrix} -\frac{i\alpha B_0}{B_0^2+B^2} & \frac{bB}{B_0^2+B^2} & 0 \\ -\frac{bB}{B_0^2+B^2}c & -\frac{i\alpha B_0}{B_0^2+B^2} & 0 \\ 0 & 0 & \alpha_{ZZ} \end{bmatrix}, \tag{5}$$

where α and b are the matrix elements of the Raman tensor without magnetic field, $B_0 = \frac{m\left(-\omega^2+i\gamma\omega+\omega_0^2\right)}{ie\omega} = g + ih$, and ω is the electric field frequency. The Raman scattering intensity at different scattering angle θ can be written as following:

$$\begin{aligned} I\left(A_g(B)\right) &\propto |e_s \cdot R \cdot e_i|^2 \\ &\propto \left| -\frac{e}{\omega}\frac{(Bb\sin\theta - h\alpha\cos\theta) + ig\alpha\cos\theta}{(g+ih)^2+B^2} \right|^2. \end{aligned} \tag{6}$$

The parameters α, b, g, and h can be obtained by fitting the experimental data. This work demonstrates that the response of the polarization axis to the magnetic field results from the magnetic control of the polarizability tensor by the Lorentz force.

In summary, these two works elucidate the rotation of the polarization axis of A_g mode (128 cm^{-1}) in CrI_3 as a function of the magnetic field from different aspects. Similar magneto-optic effects are expected in other 2D magnets, which renders them to be potentially applied to the information coding controlled by the magnetic field.[98]

4. Conclusion and perspectives

In conclusion, Raman spectroscopy is a powerful technique to study 2D magnetic materials. Besides the capability to explore the general properties related to the lattice vibration as in other 2D materials, including interlayer stacking orders, interlayer coupling, symmetry, and strain effect, Raman spectroscopy can also sensitively detect the spin-related properties of 2D magnets, like the spin-involved elementary excitation or the spin–phonon interaction.

Recent studies have found that the 2D XY-type antiferromagnetic vdW material $NiPS_3$ is a very promising magnet in 2D opto-spintronics systems. Layer-dependent Raman spectroscopy shows that the antiferromagnetism in $NiPS_3$ can be retained in the bilayer limit, while it is almost completely inhibited in the monolayer.[27] Moreover, the T_N of $NiPS_3$ flake ($N \geq 2L$) increases gradually with the number of layers. These results suggest that the XY Hamiltonian in $NiPS_3$ becomes unstable in the monolayer limit. In recent months, excitons with strong interaction between the spin and orbit are found in $NiPS_3$.[99–101] The exciton state appearing below the Néel temperature with ultra-sharp photoluminescence (PL) is gradually suppressed with the reduced thickness and eventually vanishes for the monolayer. Remarkably, an in-plane magnetic field can effectively control the optical anisotropic axis of photoluminescence along the zigzag direction. Furthermore, the existing spin-correlated excitons in $NiPS_3$ suggest that $NiPS_3$ provides an ideal system to explore the elementary photoexcitations, many-body excitons, and magneto-optics in the 2D semiconductors with intrinsic magnetic order. In particular, $NiPS_3$, which is highly sensitive to the band structure, is expected to form twisted magnetic bilayer and morié heterostructures with different vdW materials. In addition, $NiPS_3$ shows exceptionally strong exciton–phonon coupling, which provides the possibility to study the exciton–magnon coupling by optical and magnetic manipulation. Resonant Raman and Brillouin spectroscopies are also powerful techniques to investigate the exciton–phonon interaction in $NiPS_3$ and the related heterostructures.

In addition, new 2D magnets with high transition temperature above room temperature and high air stability are imperative to achieve tunable magnetism at room temperature. Large-scale growth, manageable layer number, and insensitivity under ambient conditions of vdW magnets are essential for the application of 2D magnets from lab to industry. Lacking of ferromagnetic or antiferromagnetic semiconductors is another challenge for building semiconductor spintronic devices like spin field-effect transistor. Therefore, the more precise modulation of the magnetic properties of vdW magnets, such as

the direction of magnetization, critical temperature, etc, needs to be further investigated. Additionally, the atomically sharp interface in an vdW heterostructure, which is composed of 2D magnets and other abundant vdW materials, is a new field to be explored. As one of the most convenient characterization methods of 2D magnets, Raman spectroscopy is expected to be used in more experimental work to explore the fundamental physicochemical properties of 2D magnetic vdW materials.

Considering the ultralow frequency Raman spectroscopy, which has been widely used to measure the interlayer coupling in 2D vdW materials and heterostructures, we anticipate that it will be of great use in detecting the magnetic coupling in 2D magnetic heterostructures. In much lower frequency regime below 5 cm^{-1}, we expect that the Brillouin spectroscopy will be powerful to reveal the strength of the exchange, anisotropy, topology, symmetry, and magnons in magnetic vdW materials and devices.

References

[1] Novoselov K S, Mishchenko A, Carvalho A and Castro N A H 2016 *Science* **353** aac9439

[2] Novoselov K S, Geim A K, Morozov S V, Jiang D, Zhang Y, Dubonos S V, Grigorieva I V and Firsov A A 2004 *Science* **306** 666

[3] Novoselov K S and Geim A K 2007 *Nat. Mater.* **6** 183

[4] Novoselov K S, Jiang D, Schedin F, Booth T J, Khotkevich V V, Morozov S V and Geim A K 2005 *Proc. Natl. Acad. Sci. USA* **102** 10451

[5] Liu Y, Weiss N, Duan X D, Cheng H C, Huang Y and Duan X F 2016 *Nat. Rev. Mater.* **1** 16042

[6] Zhang J 2019 *J. Semicond.* **40** 070404

[7] Samarth N 2017 *Nature* **546** 216

[8] Gong C, Li L, Li Z, Ji H, Stern A, Xia Y, Cao T, Bao W, Wang C, Wang Y, Qiu Z Q, Cava R J, Louie S G, Xia J and Zhang X 2017 *Nature* **546** 265

[9] Huang B, Clark G, Navarro-Moratalla E, Klein D R, Cheng R, Seyler K L, Zhong D, Schmidgall E, McGuire M A, Cobden D H, Yao W, Xiao D, Jarillo-Herrero P and Xu X D 2017 *Nature* **546** 270

[10] Thiel L, Wang Z, Tschudin M A, Rohner D, Gutiérrez L I, Ubrig N, Gibertini M, Giannini E, Morpurgo A F and Maletinsky P 2019 *Science* **364** 973

[11] MacNeill D, Hou J T, Klein D R, Zhang P, Jarillo H P and Liu L 2019 *Phys. Rev. Lett.* **123** 047204

[12] Yang S Q, Xu X L, Zhu Y Z, Niu R R, Xu C Q, Peng Y X, Cheng X, Jia X H, Huang Y, Xu X F, Lu J M and Ye Y 2021 *Phys. Rev. X* **11** 011003

[13] Huang B, Cenker J, Zhang X, Ray E L, Song T, Taniguchi T, Watanabe K, McGuire M A, Xiao D and Xu X D 2020 *Nat. Nanotechnol.* **15** 212

[14] Yang S X, Zhang T L and Jiang C B 2020 *Adv. Sci.* **8** 2002488

[15] Kim H H, Yang B, Patel T, Sfigakis F, Li C, Tian S, Lei H and Tsen A W 2018 *Nano Lett.* **18** 4885

[16] Li X X, Dong B J, Sun X D, Wang H W, Yang T, Yu G Q and Han Z V 2019 *J. Semicond.* **40** 081508

[17] Wang X Z, Du K Z, Fredrik L, Yu Y, Hu P, Zhang J, Zhang Q, Owen M H S, Lu X, Gan C K, Sengupta P K C and Xiong Q H 2016 *2D Mater.* **3** 031009

[18] Tian Y, Gray M J, Ji H W, Cava R J and Burch K S 2016 *2D Mater.* **3** 025035

[19] Chen W J, Sun Z Y, Wang Z J, Gu L H, Xu X D, Wu S W and Ga C L 2019 *Science* **366** 983

[20] Yang M, Li Q, Chopdekar R V, Dhall R, Turner J, Carlström J D, Ophus C, Klewe C, Shafer P, N'Diaye A T,Choi J W, Chen G, Wu Y Z, Hwang C, Wang F and Qiu Z Q 2020 *Sci. Adv.* **6** eabb5157

[21] McCreary A, Simpson J R, Mai T T, McMichael R D, Douglas J E, Butch N, Dennis C, Valdés A R and Hight W A R 2020 *Phys. Rev. B* **101** 064416

[22] Huang B, Clark G, Klein D R, MacNeill D, Navarro-Moratalla E, Seyler K L, Wilson N, McGuire M A, Cobden D H, Xiao D, Yao W, Jarillo-Herrero P and Xu X D 2018 *Nat. Nanotechnol.* **13** 544

[23] Abramchuk M, Jaszewski S, Metz K R, Osterhoudt G B, Wang Y, Burch K S and Tafti F 2018 *Adv. Mater.* **30** 1801325

[24] Sun Z, Yi Y, Song T, Clark G, Huang B, Shan Y, Wu S, Huang D, Gao C, Chen Z, McGuire M, Cao T, Xiao D, Liu W T, Yao W, Xu X D and Wu S 2019 *Nature* **572** 497

[25] Deng Y, Yu Y, Song Y, Zhang J, Wang N Z, Sun Z, Yi Y, Wu Y Z, Wu S, Zhu J, Wang J, Chen X H and Zhang Y 2018 *Nature* **563** 94

[26] Sun Y J, Tan Q H, Liu X L, Gao Y F and Zhang J 2019 *J. Phys. Chem. Lett.* **10** 3087

[27] Kim K, Lim S Y, Lee J U, Lee S, Kim T Y, Park K, Jeon G S, Park C H, Park J G and Cheong H 2019 *Nat. Commun.* **10** 345

[28] Ubrig N, Wang Z, Teyssier J, Taniguchi T, Watanabe K, Giannini E, Morpurgo A F and Gibertini M 2019 *2D Mater.* **7** 015007

[29] Lyu B, Gao Y, Zhang Y, Wang L, Wu X, Chen Y, Zhang J, Li G, Huang Q, Zhang N, Chen Y, Mei J, Yan H, Zhao Y, Huang L and Huang M 2020 *Nano Lett.* **20** 6024

[30] Fei Z, Huang B, Malinowski P, Wang W, Song T, Sanchez J, Yao W, Xiao D, Zhu X, May A F, Wu W, Cobden D H, Chu J H and Xu X D 2018 *Nat. Mater.* **17** 778

[31] Du K Z, Wang X Z, Liu Y, Hu P, Utama M I, Gan C K, Xiong Q H and Kloc C 2016 *ACS Nano* **10** 1738

[32] Li J H, Li Y, Du S Q, Wang Z, Gu B L, Zhang S C, He K, Duan W H and Xu Y 2019 *Sci. Adv.* **5** eaaw5685

[33] Otrokov M M, Klimovskikh I I, Bentmann H, *et al.* 2019 *Nature* **576** 416

[34] Aliev Z S, Amiraslanov I R, Nasonova D I, Shevelkov A V, Abdullayev N A, Jahangirli Z A, Orujlu E N, Otrokov M M, Mamedov N T, Babanly M B and Chulkov E V 2019 *J. Alloys Compd.* **789** 443

[35] Ovchinnikov D, Huang X, Lin Z, Fei Z, Cai J, Song T, He M, Jiang Q, Wang C, Li H, Wang Y, Wu Y, Xiao D, Chu J H, Yan J, Chang C Z, Cui Y T and Xu X D 2021 *Nano Lett.* **21** 2544

[36] Deng Y J, Yu Y J, Shi M Z, Guo Z X, Xu Z H, Wang J, Chen X H and Zhang Y B 2020 *Science* **367** 895

[37] Liu S H, Yuan X, Zou Y C, Sheng Y, Huang C, Zhang E, Ling J W, Liu Y W, Wang W Y, Zhang C, Zou J, Wang K Y and Xiu F X 2017 *NPJ 2D Mater. Appl.* **1** 30

[38] Li X L, Lv J T, Zhang J, You L, Su Y and Tsymbal E Y 2019 *Nano Lett.* **19** 5133

[39] May A F, Ovchinnikov D, Zheng Q, Hermann R, Calder S, Huang B, Fei Z, Liu Y, Xu X D and McGuire M A 2019 *ACS Nano* **13** 4436

[40] Park S Y, Kim D S, Liu Y, Hwang J, Kim Y, Kim W, Kim J Y, Petrovic C, Hwang C, Mo S K, Kim H J, Min B C, Koo H C, Chang J, Jang C, Choi J W and Ryu H 2020 *Nano Lett.* **20** 95

[41] Drachuck G, Salman Z, Masters M W, Taufour V, Lamichhane T, Lin Q S, Straszheim W E, Bud'ko S L and Canfield P C 2018 *Phys. Rev. B* **98** 144434

[42] Huang B, McGuire M A, May A F, Xiao D, Jarillo H P and Xu X D 2020 *Nat. Mater.* **19** 1276

[43] Zhong D, Seyler K L, Linpeng X, Wilson N P, Taniguchi T, Watanabe K, McGuire M A, Fu K C, Xiao D, Yao W and Xu X D 2020 *Nat. Nanotechnol.* **15** 187

[44] Susner M A, Chyasnavichyus M, McGuire M A, Ganesh P and Maksymovych P 2017 *Adv. Mater.* **29** 1602852

[45] Coak M J, Jarvis D M, Hamidov H, Wildes A R, Paddison J A M, Liu C, Haines C R S, Dang N T, Kichanov S E, Savenko B N, Lee S, Kratochvílová M, Klotz S, Hansen T C, Kozlenko D P, Park J G and Saxena S S 2021 *Phys. Rev. X* **11** 011024

[46] Lee J U, Lee S, Ryoo J H, Kang S, Kim T Y, Kim P, Park C H, Park J G and Cheong H 2016 *Nano Lett.* **16** 7433

[47] Kuo C T, Neumann M, Balamurugan K, Park H J, Kang S, Shiu H W, Kang J H, Hong B H, Han M, Noh T W and Park J G 2016 *Sci. Rep.* **6** 20904

[48] Xing W Y, Qiu L Y, Wang X R, Yao Y Y, Ma Y, Cai R, Jia S, Xie X C and Han W 2019 *Phys. Rev. X* **9** 011026

[49] Cong X, Liu X L, Lin M L and Tan P H 2020 *NPJ 2D Mater. Appl.* **4** 13

[50] Cenker J, Huang B, Suri N, Thijssen P, Miller A, Song T C, Taniguchi T, Watanabe K, McGuire M A, Xiao D and Xu X D 2020 *Nat. Phys.* **17** 20

[51] Li T, Jiang S, Sivadas N, Wang Z, Xu Y, Weber D, Goldberger J E, Watanabe K, Taniguchi T, Fennie C J, Fai M K and Shan J 2019 *Nat. Mater.* **18** 1303

[52] Cong X, Lin M L and Tan P H 2019 *J. Semicond.* **40** 091001

[53] Li T H, Zhou Z H, Guo J H and Hu F R 2016 *Chin. Phys. Lett.* **33** 046201

[54] Liang F, Xu, H J, Wu X, Wang C L, Luo C and Zhang J 2018 *Chin. Phys. B* **27** 037802

[55] Zhang C, Chen B Q and Li Z Y 2016 *Chin. Phys. B* **25** 095203

[56] Yang Q, Xue Y Z, Chen H, Dou, X M and Sun B Q 2020 *J. Semicond.* **41** 082004

[57] Tan P H 2019 *Raman Spectroscopy of Two-Dimensional Materials* (Singapore: Springer) p. 276

[58] Liang L, Zhang J, Sumpter B G, Tan Q H, Tan P H and Meunier V 2017 *ACS Nano* **11** 11777

[59] Devereaux T P and Hackl R 2007 *Rev. Mod. Phys.* **79** 175

[60] Wan J W, Guo J H and Hu F R 2017 *J. Semicond.* **38** 042003

[61] Ferrari A C and Basko D M 2013 *Nat. Nanotechnol.* **8** 235

[62] Tan Q H, Sun Y J, Liu X L, Xu K X, Gao Y F, Ren S L, Tan P H and Zhang J 2020 *Nano Res.* **14** 239

[63] Tan Q H, Sun Y J, Liu X L, Zhao Y Y, Xiong Q H, Tan P H and Zhang J 2017 *2D Mater.* **4** 031007

[64] Nasu J, Knolle J, Kovrizhin D L, Motome Y and Moessner R 2016 *Nat. Phys.* **12** 912

[65] Tan P H, Han W P, Zhao W J, Wu Z H, Chang K, Wang H, Wang Y F, Bonini N, Marzari N, Pugno N, Savini G, Lombardo A and Ferrari A C 2012 *Nat. Mater.* **11** 294

[66] Liu X L, Zhang X, Lin M L and Tan P H 2017 *Chin. Phys. B* **26** 067802

[67] Kim J, Lee J U and Cheong H 2020 *J. Phys. Condens. Matter* **32** 343001

[68] Talochkin A B 2019 *J. Raman Spectrosc* **51** 201

[69] Tian X Y and Liu Y S 2021 *J. Semicond.* **42** 032001

[70] Zhang T, Wang Y, Li H, Zhong F, Shi J, Wu M, Sun Z, Shen W, Wei B, Hu W, Liu X, Huang L, Hu C, Wang Z, Jiang C, Yang S, Zhang Q M and Qu Z 2019 *ACS Nano* **13** 11353

[71] Tian S, Zhang J F, Li C, Ying T, Li S, Zhang X, Liu K and Lei H 2019 *J. Am. Chem. Soc.* **141** 5326

[72] Lin M W, Zhuang H L, Yan J Q, Ward T Z, Puretzky A A, Rouleau C M, Gai Z, Liang L B, Meunier V, Sumpter B G, Ganesh P, Kent P R C, Geohegan D B, Mandrus D G and Xiao K 2016 *J. Mater. Chem. C* **4** 315

[73] McGuire M A, Dixit H, Cooper V R and Sales B C 2015 *Chem. Mater.* **27** 612

[74] Kozlenko D P, Lis O N, Kichanov S E, Lukin E V, Belozerova N M and Savenko B N 2021 *npj Quantum Mater.* **6** 19

[75] Kim H H, Yang B, Li S, Jiang S, Jin C, Tao Z, Nichols G, Sfigakis F, Zhong S, Li C, Tian S, Cory D G, Miao G X, Shan J, Mak K F, Lei H, Sun K, Zhao L and Tsen A W 2019 *Proc. Natl. Acad. Sci. USA* **116** 11131

[76] Kong T, Stolze K, Timmons E I, Tao J, Ni D, Guo S, Yang Z, Prozorov R and Cava R J 2019 *Adv. Mater.* **31** 1808074

[77] Casto L D, Clune A J, Yokosuk M O, Musfeldt J L, Williams T J, Zhuang H L, Lin M W, Xiao K, Hennig R G, Sales B C and Yan J Q, Mandrus D 2015 *APL Mater.* **3** 041515

[78] Du L J, Tang J, Zhao Y C, Li X M, Yang R, Hu X R, Bai X Y, Wang X, Watanabe K J, Taniguchi T, Shi D X, Yu G Q, Bai X D, Hasan T, Zhang G Y and Sun Z P 2019 *Adv. Funct. Mater.* **29** 1904734

[79] Chen B, Yang J H, Wang H D, Imai M, Ohta H, Michioka C, Yoshimura K and Fang M H 2013 *J. Phys. Soc. Jpn.* **82** 124711

[80] Kiichi O, Ko K, Shozo S, Makoto H, Zhihong Y and Muneyuky D 1986 *J. Phys. Soc. Jpn.* **55** 4456

[81] Wildes A R, Simonet V, Ressouche E, McIntyre G J, Avdeev M, Suard E, Kimber S A J, Lançon D, Pepe G, Moubaraki B and Hicks T J 2015 *Phys. Rev. B* **92** 224408

[82] Mai T T, Garrity K F, McCreary A, Argo J, Simpson J R, Doan N V, Valdes A R and Hight W A R 2020 arXiv: 2011.12557 [cond-mat.mtrl-sci]

[83] Jin W, Kim H H, Ye Z, Li S, Rezaie P, Diaz F, Siddiq S, Wauer E, Yang B, Li C, Tian S, Sun K, Lei H, Tsen A W, Zhao L and He R 2018 *Nat. Commun.* **9** 5122

[84] Fleury P A and Loudon R 1968 *Phys. Rev.* **166** 514

[85] Fleury P A, Porto S P S, Cheesman L E and Guggenheim H J 1966 *Phys. Rev. Lett.* **17** 84

[86] Ohlmann R C and Tinkham M 1961 *Phys. Rev.* **123** 425

[87] Fleury P A 1969 *Phys. Rev.* **180** 591

[88] Johnson F M and Nethercot A H 1959 *Phys. Rev.* **114** 705

[89] Venugopalan S, Petrou A, Galazka R R, Ramdas A K and Rodriguez S 1982 *Phys. Rev. B* **25** 2681

[90] White R M, Nemanich R J and Tsang C 1980 *J. Magn. Magn. Mater.* **15–18** 773

[91] Liu S, Aguila A G, Bhowmick D, Gan C K, Do T H, Prosnikov M A, Sedmidubsky D, Sofer Z, Christianen P C M, Sengupta P and Xiong Q H 2021 *Phys. Rev. Lett.* **127** 097401

[92] Vaclavkova D, Palit M, Wyzula J, Ghosh S, Delhomme A, Maity S, Kapuscinski P, Ghosh A, Veis M, Grzeszczyk M, Faugeras C, Orlita M, Datta S and Potemski M 2020 arXiv: 2108.10945v3 [cond-mat.mtrl-sci]

[93] Wang Z, Zhang T, Ding M, Dong B, Li Y, Chen M, Li X, Huang J, Wang H, Zhao X, Li Y, Li D, Jia C, Sun L, Guo H, Ye Y, Sun D, Chen Y, Yang T, Zhang J, Ono S, Han Z and Zhang Z 2018 *Nat. Nanotechnol.* **13** 554

[94] Song T, Fei Z, Yankowitz M, Lin Z, Jiang Q, Hwangbo K, Zhang Q, Sun B, Taniguchi T, Watanabe K, McGuire M A, Graf D, Cao T, Chu J H, Cobden D H, Dean C R, Xiao D and Xu X D 2019 *Nat. Mater.* **18** 1298

[95] Fert A, Reyren N and Cros V 2017 *Nat. Rev. Mater.* **2** 17031

[96] Verzhbitskiy I A, Kurebayashi H, Cheng H X, Zhou J, Khan S, Feng Y P and Eda G 2020 *Nat. Electron.* **3** 460

[97] McCreary A, Mai T T, Utermohlen F G, Simpson J R, Garrity K F, Feng X, Shcherbakov D, Zhu Y, Hu J, Weber D, Watanabe K, Taniguchi T, Goldberger J E, Mao Z, Lau C N, Lu Y, Trivedi N, Valdes A R and Hight W A R 2020 *Nat. Commun.* **11** 3879

[98] Liu Z, Guo K, Hu G, Shi Z, Li Y, Zhang L, Chen H, Zhang L, Zhou P, Lu H, Lin M L, Liu S, Cheng Y, Liu X L, Xie J, Bai L, Tan P H, Deng L, Qiu C W and Peng B 2020 *Sci. Adv.* **6** eabc7628

[99] Wang X Z, Cao J, Lu Z G, Cohen A, Kitadai H, Li T S, Tan Q S, Wilson M, Lui C H, Smirnov D, Sharifzadeh S and Ling X 2021 *Nat. Mater.* **20** 964

[100] Hwangbo K, Zhang Q, Jiang Q, Wang Y, Fonseca J, Wang C, Diederich G M, Gamelin D R, Xiao D, Chu J H, Yao W and Xu X D 2021 *Nat. Nanotechnol.* **16** 655

[101] Kang S, Kim K, Kim B H, Kim J, Sim K I, Lee J U, Lee S, Park K, Yun S, Kim T, Nag A, Walters A, Garcia F M, Li J, Chapon L, Zhou K J, Son Y W, Kim J H, Cheong H and Park J G 2020 *Nature* **583** 785